Control Mitigation for Over-Speeding in Curves: Strategies to Minimize Off-Tracking

Citation for the original published paper (version of record):

Gordon, T., Klomp, M., Lidberg, M. (2012). Control Mitigation for Over-Speeding in Curves: Strategies to Minimize Off-Tracking. Proceedings of the 11th International Symposium on Advanced Vehicle Control (AVEC '12)

N.B. When citing this work, cite the original published paper.

(article starts on next page)

Strategies for Minimizing Maximum Off-tracking resulting from Over-speed in Curves

Tim J Gordon[1], Matthijs Klomp[2] & Mathias Lidberg[3]

[1]University of Michigan, Mechanical Engineering

Ann Arbor, MI 48109-2121, USA, e-mail: tjgordon@umich.edu

[2]eAAM Driveline Systems, Vehicle Dynamics and Control

SE-461 54 Trollhättan, Sweden, e-mail: matthijs.klomp@aam.com

[3]Chalmers University of Technology, Vehicle Dynamics

SE-412 96 Gothenburg, Sweden, e-mail: mathias.lidberg@chalmers.se

This paper tests the effectiveness of closed-loop brake control to reduce vehicle off-tracking arising from over-speeding in curves. When a driver enters a curve too fast given the available friction, the aim is to use electronic brake control to reduce speed and increase path curvature to complete the turn. Previously it has been found that coordinated four wheel braking referenced to an inertially fixed vehicle mass center acceleration (PPR) is an optimal control strategy. The present work introduces the effect of driver-vehicle interaction, using simulation and track experiments. It is confirmed that PPR effectiveness is not disrupted by typical steering corrections from the driver. PPR is found to offer significant path following improvements compared with other brake control strategies.

1 INTRODUCTION

In this paper we consider the problem of terminal understeer in curves. In accident statistics [1, 2] this is recognized as a situation where curve entry speed is too high for the required path curvature, given the prevailing tire/road friction; as a result the vehicle follows a wider path than desired, incurring multiple risks associated with unintended lane or road departure. To minimize such risk it is proposed to apply brake forces in an optimal sense, which we formulate as the minimization of maximum pat off-tracking, i.e. minimizing the worst-case deviation from intended path.

In the literature [3, 4, 5] much more attention has been paid to yaw stability in curves than on path off-tracking. In fact, yaw stability is rarely an issue for overspeed in curves due to saturation of the front lateral tire forces, a stable condition of the vehicle. If yaw instability occurs, it is controlled by the direct application of braking forces to generate yaw moments acting in the opposite sense to the direction of turn, simultaneously reducing excessive yaw rate and body side-slip. A common assumption is that understeer mitigation is the direct opposite of oversteer mitigation, and hence yaw moments should be applied in the *same* direction as the turn in order to increase yaw rate [4, 5]. While it is true this will increase vehicle heading angle in the turn direction, there is no guarantee that it will simultaneously increase path curvature, especially when operating at the friction limits.

In the following an optimal strategy is developed based on a simple particle representation of the vehicle dynamics. In previous research [6, 7] it was shown that the optimal particle response to off-tracking due to friction limits is in the form of a *parabolic path recovery* (PPR), and that numerical optimization for off-tracking minimization with a nonlinear vehicle handling model shows very similar response characteristics. Here the essential elements of this optimal open-loop control are used to develop a closed-loop brake controller that can be implemented in simulation and in a test vehicle, including closed-loop response from the driver. The longitudinal dynamics of the optimal particle response (the speed profile) is used as the primary reference for the closed-loop trajectory control; by maintaining maximum available acceleration at the mass center, the lateral acceleration and path in space are expected to closely match the ideal PPR solution, as in [6].

While earlier research [6, 7] was directed at the performance evaluation of PPR using simple open-loop control inputs, in the present analysis we consider driver intention and interaction as crucial to the system evaluation. In particular we expect a normal driver to respond to terminal understeer by steadily increasing the steering wheel angle during the turn event in an effort to increase the path curvature. In an uncontrolled vehicle this may be counter-productive since beyond the front tire adhesion limits this will typically reduce the cornering force and increase the degree of understeer. In this case PPR will automatically apply progressive speed reductions; so PPR control will not only reduce off-tracking (based on previous research), it is also anticipated to help maintain the connection between path curvature and steering wheel angle *beyond the normal grip limits* in a way that is not possible with the passive vehicle dynamics.

For the purpose of comparing the two fundamentally different approaches to understeer mitigation, we implement the following in both simulation and experiment: (a) a speed-based feedback control version of PPR, which essentially controls the direction of the mass center acceleration vector; (b) a yaw rate feedback control (called DYC) which focuses instead on yaw-moment control. The DYC controller is based on published literature to brake only the inner wheels. While more sophisticated understeer mitigation algorithms may be implemented in commercial systems, these include many heuristic control rules, and are not available in the public domain. More importantly, it is beneficial to compare clearly distinguished control concepts to evaluate their inherent differences.

In Section 2.1 we introduce a simple non-linear two-track model representing the vehicle dynamics characteristics of a typical passenger vehicle, while in Section 2.2 a simple driver model is defined for use in simulation. In Section 3 the path tracking task is defined relative to an inferred reference path. In Section 3.1 this is formalized as an optimal control problem and an explicit closed-form solution is found for a simple particle motion in Section 3.2. Section 4 introduces a simple driver interpreter and its connection to the two closed-loop control strategies, one based on the PPR concept and one based on DYC. The controllers are evaluated in Section 5, first in simulation and secondly from track tests. Finally, Section 6 provides conclusions of the work, and appendices present supporting model parameter data as well as a full derivation of the closed-form optimal control strategy.

2 SIMULATION MODELS

In this section a vehicle model and a driver model are presented. We assume each wheel is capable of individual wheel braking, controlled through solenoid valves. Required sensors are for steering angle, lateral acceleration and yaw rate, all commonly available in commercial stability control systems.

2.1 Vehicle Model

The two-track vehicle model is shown in Figure 1. The model assumes front steering with equal angles at the left and right wheels. The longitudinal tire forces, F_{Xij}, which are individually controlled, we have that i is the index for the front/rear wheels and j for the left/right wheels. In the figure, part of the notation used for the modeling is shown. Note that both traction and braking forces are permitted; when we consider the results we will conclude whether braking only is sufficient. The lateral tire forces, F_{Yij}, are modeled as a function of the vehicle states, the front steering angle and brake inputs [7].

The following state-space model, using motion variables in the vehicle fixed $X - Y$ reference frame is derived
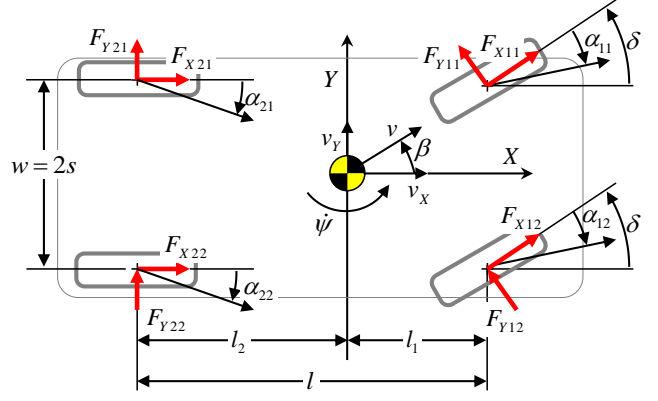

Figure 1: Two-track vehicle model. The arrows show the positive direction of each angle or force.

from Newton's second law of motion:

$$m(\dot{v}_X - v_Y\dot{\psi}) = \sum_{i,j} \bar{F}_{Xij}$$

$$m(\dot{v}_Y + v_X\dot{\psi}) = \sum_{i,j} \bar{F}_{Yij}$$

$$mk^2\ddot{\psi} = \sum_{i,j}((-1)^j s\bar{F}_{Xij} - (-1)^i l_i\bar{F}_{Yij}) \quad (1)$$

$$\dot{x}_c = v_X\cos\psi - v_Y\sin\psi$$

$$\dot{y}_c = v_X\sin\psi + v_Y\cos\psi$$

where $\bar{F}_{Xij}$ and $\bar{F}_{Yij}$ are the respective longitudinal and lateral wheel forces resolved in the local vehicle reference frame, m the total vehicle mass and k is the radius of gyration. The vertical forces, F_{Zij}, are a result of the static load distribution and the load transfer due to the longitudinal and lateral acceleration. This results in the following model of the tire vertical force:

$$F_{Zij} = \zeta_{0i}mg + (-1)^i\zeta_X ma_X + (-1)^j\zeta_{Yi}ma_Y \quad (2)$$

where, g, a_X and a_Y are the gravitational, vehicle longitudinal and lateral acceleration, respectively, $\zeta_{0i} = (l - l_i)/(2l)$ is the static force distribution coefficient, $\zeta_X = h/(2l)$ is the longitudinal load transfer coefficient and ζ_{Yi} is the lateral load transfer coefficient of each axle, h is the height of mass center above the ground. The lateral load transfer coefficient is a lumped parameter taking the roll stiffness distribution, roll center heights, etc. into account and it is available together with other vehicle data in Appendix A.

2.2 Driver Model

The driver model used in this paper steers toward a preview point with a preview curvature κ_p (see Figure 2) such that

$$\delta = l\kappa_p + \mu_0 gK\text{atanh}\left(\frac{\kappa_p v^2}{\mu_0 g}\right), \quad |\kappa_p v^2| < \mu_0 g \quad (3)$$

where K is the understeer gradient of the vehicle, determined from a steady-state circular driving maneuver. The curvature from the vehicle position (x_c, y_c) in the direction
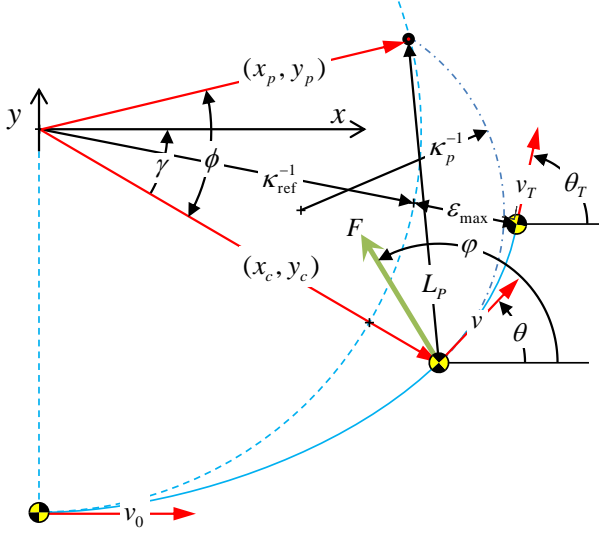
Figure 2: Notation used to determine the position of the vehicle (x_c, y_c) relative to the reference trajectory in the global coordinate system. Additionally the position of the preview point (x_p, y_p), used for the driver model, at a preview distance L_p is shown.

of the vehicle velocity vector φ toward the preview point (x_p, y_p) can be determined to be

$$\kappa_p = 2\frac{(x_c - x_p)\sin\theta - (y_c - y_p)\cos\theta}{(x_c - x_p)^2 + (y_c - y_p)^2} \qquad (4)$$

The preview point is unknown but lies on the track at a preview distance L_p from the vehicle position:

$$\begin{aligned} x_p &= \kappa_{\text{ref}}^{-1}\cos(\phi + \gamma) \\ y_p &= \kappa_{\text{ref}}^{-1}\sin(\phi + \gamma) \end{aligned} \qquad (5)$$

The preview distance (or preview horizon) is velocity dependent such that

$$L_p = L_{p0} + T_p v \qquad (6)$$

where L_{p0} is the minimum preview distance and T_p is the preview time horizon. For the simulations in this paper $L_{p0} = 5$ m and $T_p = 2$ s.

3 UNDERSTEER MITIGATION AS AN OPTIMAL CONTROL PROBLEM

As discussed in the introduction, the aim for the driver is to follow a desired path while maintaining sufficient yaw stability. In this section, the optimal recovery from terminal understeer is defined as a optimal control problem of minimizing the maximum deviation from the previously inferred reference curve. Subsequently, a closed-form optimal control solution for simple particle motion is presented which will be used as reference for a subsequent closed-loop controller synthesis.

3.1 Recovery from Terminal Understeer as an Optimal Control Problem

In this formulation we simplify the driver input to be a step-steer, and hence the inferred path is a circular arc – see Section 4.1 below. Let the circular arc have curvature κ_{ref}. From this curvature and the friction limit μ the corresponding maximum achievable speed can be determined as:

$$v_{\text{lim}} = \sqrt{\mu g |\kappa_{\text{ref}}^{-1}|} \qquad (7)$$

In the case of excessive initial speed, $v_0 > v_{\text{lim}}$, the actual vehicle trajectory will deviate from the reference trajectory. Thus with initial conditions

$$x_c(0) = 0, \quad y_c(0) = -\kappa_{\text{ref}}^{-1}, \quad \dot{x}_c(0) = v_0, \quad \dot{y}_c(0) = 0 \quad (8)$$

the optimal control problem is to minimize

$$J = x_c^2(T) + y_c^2(T) \qquad (9)$$

subject to the following condition at $t = T$:

$$x_c(T)\dot{x}_c(T) + y_c(T)\dot{x}_c(T) = 0 \qquad (10)$$

i.e. the velocity vector is perpendicular to the radial vector from the center of the circle at the final time.

3.2 Optimal Control for a Particle Representation

For this particular problem, stable yaw motion but terminal understeer resulting in path off-tracking, the dynamics of the problem may be simplified to a point-mass representation. This means that the yaw degree of freedom of Equation (1) is omitted (since it is assumed to be stable) and then subsequently describing the motion of the vehicle as a point-mass particle moving in the X_E-Y_E reference frame, as shown in Figure 2.

The motivation for the particle representation is to be able to analytically derive an optimal strategy for recovery from terminal understeer. This way of representing the dynamics of the vehicle under terminal understeer condition also provides greater insight into the fundamentals of the recovery from terminal understeer.

By summing up the tire forces into a single force vector and approximating the combined force capacity of all tires with a single friction circle, the lateral and longitudinal equations of motion from Equation (1) can be expressed in the inertial reference frame as:

$$\begin{aligned} \ddot{x}_c &= F/m\cos\varphi \\ \ddot{y}_c &= F/m\sin\varphi \end{aligned} \qquad (11)$$

where $|F| < \mu g$.

The recovery from terminal understeer problem of minimizing the maximum off-tracking distance is solved in [8]. There the optimal control input, $(F^*(t), \varphi^*(t))$, is shown to be constant

$$\begin{aligned} F^*(t) &= \mu mg \\ \varphi^*(t) &= \pi/2 + \theta_T \end{aligned} \qquad (12)$$

The optimal control (12) implies that for all $t \in [0,T]$ the force is constant at the friction limit with a globally fixed direction perpendicular to the velocity vector at the time T of maximum deviation. From the optimal control $(F^*(t), \varphi^*(t))$ it follows that optimal recovery from terminal understeer trajectory is equivalent to a classic parabolic projectile motion, henceforth called the parabolic path recovery (PPR) from terminal understeer strategy.

The velocity of the particle for the optimal control input, is obtained by integration of the model (11) using $(F^*(t), \varphi^*(t))$ and the initial values in Equation (8) such that

$$\begin{aligned} \dot{x}_c &= v_0 - \mu g t \sin\theta_T \\ \dot{y}_c &= \mu g t \cos\theta_T \end{aligned} \tag{13}$$

From these equations we find that

$$\cos\theta_T = (v_{\mathrm{lim}}/v_0)^2 \tag{14}$$

where $\theta_T = \theta(T)$, see also Figure 2. Further, the time of maximum off-tracking (final time in the optimization) is found from Equation (11) as the time it takes for the velocity perpendicular to θ_T to reach zero

$$T = v_0 \sin\theta_T / (\mu g) \tag{15}$$

The final speed of the particle is obtained by computing the magnitude of Equation (13) and combine with Equation (15) to give that

$$v(T) = v_{\mathrm{lim}}^2 / v_0 \tag{16}$$

which is an important result that will be used later to develop a closed-loop control strategy for understeer control.

Although not reported in this paper, it was confirmed in [7] that very similar results as those for the particle are found when applying optimal control to the vehicle model described in Section 2.1. This confirmed that for this particular problem, stable yaw motion and operating at the limit of adhesion, that important conclusions about how to solve the path off-tracking resulting from terminal understeer may be addressed. This will be utilized in the controller synthesis in the next section.

4 Controller Synthesis

4.1 Driver Interpreter

A simple driver interpreter is assumed [9, 5], based on a linear bicycle model without time delay. The desired path curvature, κ_{ref}, may be found from the steering wheel input to the steady-state path curvature gain

$$\kappa_{\mathrm{ref}} = \frac{\delta_H}{i_S} \frac{1}{l + K v^2} \tag{17}$$

where i_S is the ratio between δ_H and the (mean) road wheel angle δ of the front wheels and K is the understeer gradient. This is given to be specific; in fact, the precise form of the interpreter does not affect the details of our subsequent analysis.

4.2 Closed-loop PPR

In Section 3.2 it was shown that, for a particle representation of the terminal understeer problem, the optimal control with respect to a circular reference is a parabolic path. Also, the open-loop optimal control for the two-track vehicle model was obtained in [7] and found to closely match the trajectory and speed profile of the particle representation. Can a closed-loop controller be obtained to mimic the behavior of open-loop optimal control solution?

From Equation (16) it can be seen that the final speed for the open-loop optimal control for a particle is v_{lim}^2/v_0. This speed could be a good reference for a closed-loop speed controller. Nevertheless, although v_{lim} can be inferred from the steering wheel input if the a fair estimate of the road friction exists, v_0 can only be remembered if the steering input remains constant throughout the entire maneuver. For this reason our first implementation of PPR aims to achieve v_{lim} as the target speed. It is also implied that if less speed than v_{lim} is demanded by the driver for a given steering input, the driver can simply change this by steering more.

Based on the discussion above, it thus proposed to use a proportional controller on the speed difference between limit speed v_{lim} and the current speed. The control law therefore is proposed to be such that the brake forces should be applied using the following proportional control law

$$F_{Xij}(t) = -\gamma_{ij} \max(v(t) - v_{\mathrm{lim}}, 0) \tag{18}$$

Note that the max statement ensures that braking only occurs for $v > v_{\mathrm{lim}}$. The target speed v_{lim} is computed from Equation (7) using an estimated coefficient of friction.

In the simulations $\mu = 0.70$, $\gamma_{11} = 1.1 \cdot 10^4$, $\gamma_{12} = 0.45 \cdot 10^4$, $\gamma_{21} = 0.45 \cdot 10^4$ and $\gamma_{11} = 1.1 \cdot 10^4$. It may be noted that this implies more braking on the *outer* wheels, which is contrary to the strategy proposed for yaw moment control.

4.3 DYC Understeer Control

It is of interest to know how the PPR strategy compares to the standard direct yaw moment control (DYC) method based on inner-wheel(s) braking [5], which is the strategy most often proposed in the literature for understeer control. To recover from understeer via DYC it is suggested to apply a turn-in yaw moment by braking the inner rear wheel. However, care must be taken not to overbrake the single wheel since this can lead to excessive side-slip [9]. Initial simulations determined that braking both inner wheels was more effective than braking only the inner rear wheel (also proposed in reference [5]) so this modification is implemented to improve the performance of the yaw moment control in our comparison. In our implementation of this strategy the longitudinal force vector is:

$$F_{Xij}(t) = -\gamma_{ij} \max(|v_X \kappa_{\mathrm{ref}}| - |\dot{\psi}|, 0) \tag{19}$$

where for a left turn ($\dot{\psi} > 0$) we have that $\gamma_{12} = \gamma_{22} = 0$ (inner wheels braking only). These parameters are tuned to $\gamma_{11} = 4.2 \cdot 10^7$ and $\gamma_{21} = 2.7 \cdot 10^7$, to be roughly similar to what would be achieved by the method proposed in [5].

5 CONTROLLER EVALUATION

The controller was developed using mainly simulations but the effectiveness was evaluated under realistic conditions using experiments on the test track. The experiments were only performed on dry asphalt, although even more benefit from this type of control is anticipated on low-friction surfaces. Future work should of course also include experiments on these surfaces.

5.1 Over-Speed in Curve Maneuver

The experimental setup both for simulations and experiments is shown in Figure 3 where two semi-circles are used to mark the reference trajectory. The lower semicircle is used for left-hand turns and the upper circle for turning in the opposite direction. Only one of them is used as reference to compute the off-tracking distance.
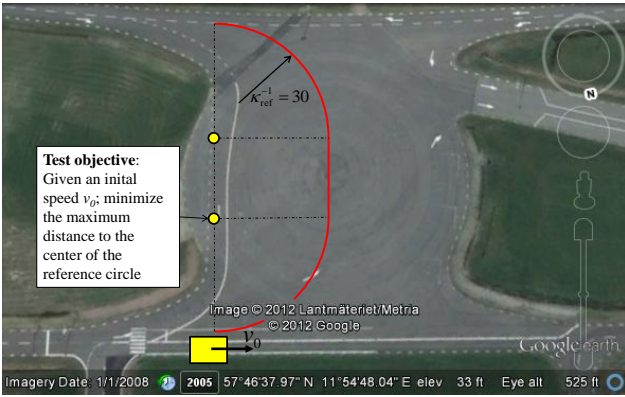
Figure 3: Over-speed in curve maneuver. Image ©2012 Lantmäteriet/Metria and ©2012 Google.

5.2 Simulation Results

Simulation results are shown in Figures 4-5. In Figure 4, the trajectories for the three different strategies are shown and it can be seen that PPR strategy recovers the reference path first. In Figure 5 the speed and v_{lim} (dashed lines) are shown in (a), the side-slip angle versus time in (b), the yaw rate and reference yaw rate (dashed lines) in (c), the path off-tracking in (d), the acceleration magnitude in (e), and the steering wheel angle in (f) are shown for the three different strategies. By comparing (a) and (d) it appears a clear correlation between the maximum off-tracking and an early reduction in vehicle speed. For this purpose, braking all four wheels is naturally more efficient than using only two wheels.
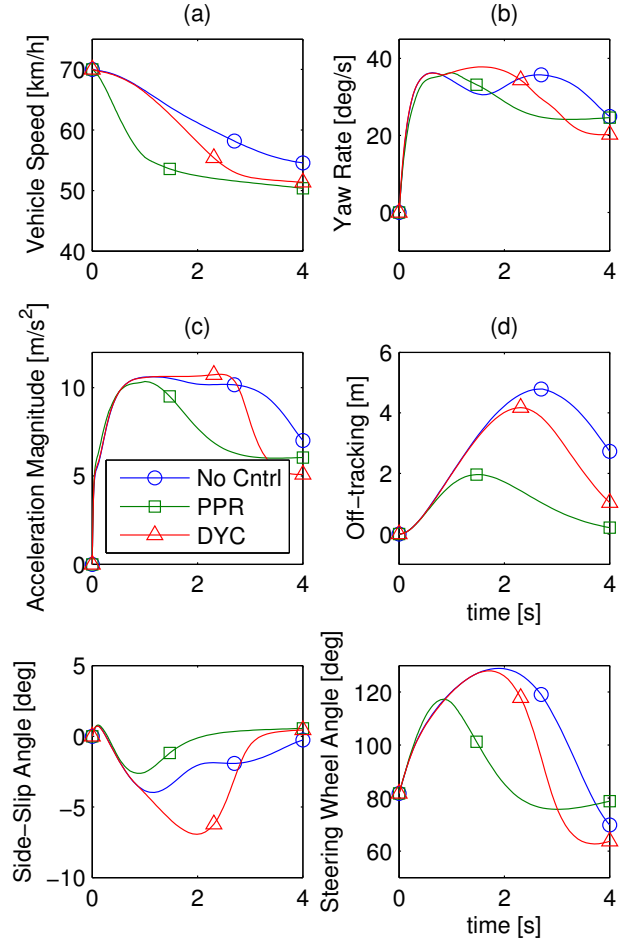
Figure 4: Vehicle states as function of time. The intermediate markers indicate the point of maximum off-tracking.
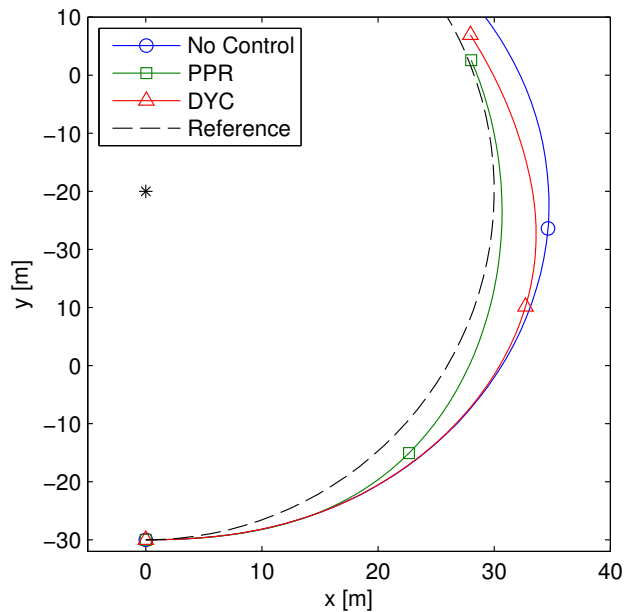
Figure 5: Trajectories of the different control strategies for the performed simulations. The intermediate markers indicate the point of maximum off-tracking.

5.3 Experimental Results

The experimental vehicle shown in Figure 6 is a front-wheel-drive 2009 Saab 9-3 with a 250hp V6 engine and a six-speed manual transmission. The vehicle is equipped with an additional four identical brake calipers controlled via an electro-hydraulic brake (EHB) system. For more details about the test vehicle, see [10].

Figure 6: Test vehicle (Saab 9-3)

The experiments are conducted such that the driver enters the course at a given initial speed v_0 and then attempts to minimize the maximum distance to the reference trajectory. For the circle, this is equivalent to minimizing the maximum off-tracking from the center of the semicircle. The experiments were performed on dry asphalt with the driver's aim to following a circular reference trajectory. The reference path with $\kappa_{\mathrm{ref}}^{-1} = 30$ m with $v_{\mathrm{lim}} \approx 55$ km/h, all experiments were conducted at $v_0 = 70$ km/h.

The same two closed-loop control algorithms presented in the previous section (PPR and DYC) were implemented in a real-time computer in the test-vehicle and compared to the uncontrolled case. The results from these experiments can be seen in Figure 7 and Figure 8. There it can be seen that qualitatively the same results are observed from experiments as from simulations. For the uncontrolled vehicle it was noted that, as expected, very small differences in off-tracking were found for $90°$ steering wheel input and $180°$ until the tires have recovered from saturation. What this implies is that the driver is out of control since doubling the steering input has little effect on the path. The DYC algorithm does improve the path tracking, but the rapid increase in side-slip angle was subjectively felt as very uncomfortable. The initial implementation of the PPR algorithm, presented in this paper, gave the driver an additional degree of freedom through the steering wheel by braking as function of steering wheel input when the lateral tire forces become saturated. By this, the driver is put back into control by controlling the speed and path in an intuitive way and, when the brake controller deactivates, gives the normal steering control back to the driver, which was lost when the lateral tire forces were saturated.
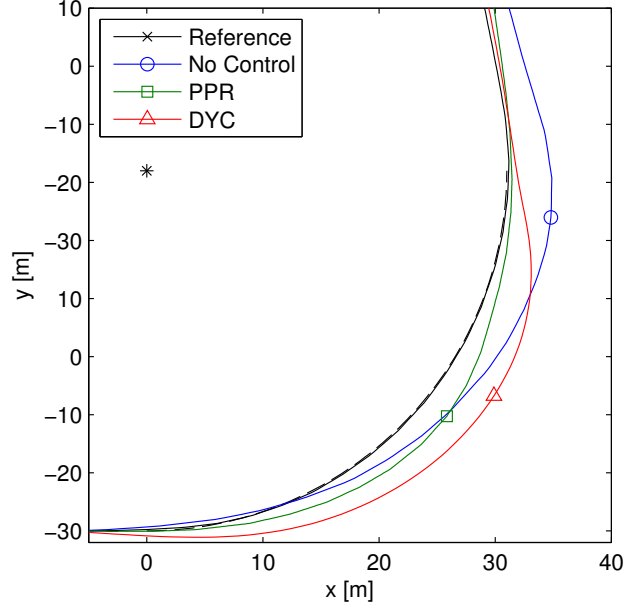

Figure 7: Trajectories of the different control strategies for the performed experiments. The intermediate markers indicate the point of maximum off-tracking.
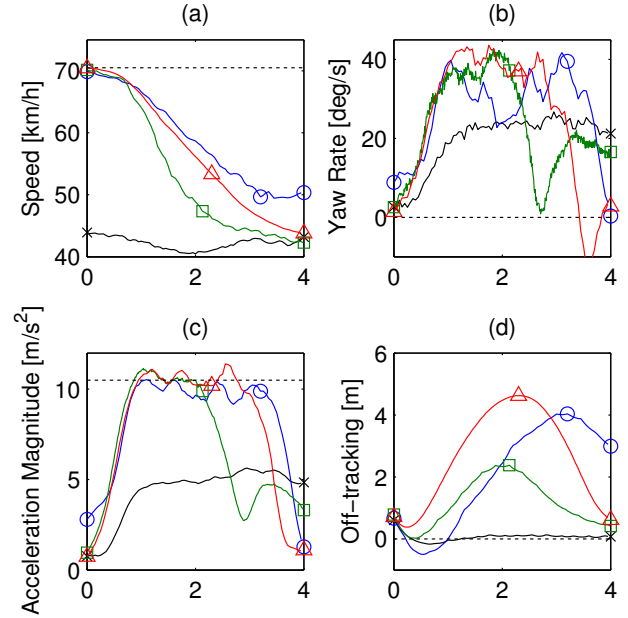

Figure 8: Vehicle states as function of time. The intermediate markers indicate the point of maximum off-tracking.

6 CONCLUSIONS

Since terminal understeer can cause run-off road crashes, the problem of terminal understeer is here formulated as a problem to minimize the maximum off-tracking (deviation) from an intended path. This problem is addressed in two different ways: A standard direct yaw-moment control (DYC) based method and a second method using the essence of the optimal control results for the particle representation. A comparison of the two methods led to the conclusion that speed control is more important than yaw-moment control and therefor an early speed reduction is more efficient than increasing yaw rate. The first contribution of this paper is the formulation as the problem of terminal understeer as an off-tracking minimization problem. Secondly, a closed-form optimal solution for a particle representation of the off-tracking problem was shown. Furthermore, a simple closed-loop controller was developed which aims to slow the speed down to the maximum speed achievable for the curvature inferred from the driver's steering input. This controller, and a yaw-moment control strategy from the literature, were evaluated both in simulation and during experiments on high-mu surfaces.

The control design proposed in this paper is, however, very preliminary and requires more work in future research. One main difference between the developed closed-loop controller and an optimal control solution for a particle representation of the terminal understeer problem, is that the target speed is v_{lim} instead of v_{lim}^2/v_0 for the latter. The reason for this is that the initial speed, v_0, can only be remembered if the steering angle remains unchanged throughout the event. One way to alleviate the reliance on the steering input to infer the target path curvature is to use environmental sensors. Also this is a topic for further research.

Even though the closed-loop controller proposed in this paper is only in the early stages of development, both simulation results and experiments confirm that moving away from the classic direct yaw moment control approach to controlling the acceleration vector is much more important when it comes to reducing the off-tracking from a reference trajectory.

ACKNOWLEDGEMENTS

References

[1] Cejun Liu and Rajesh Subramanian. Factors related to fatal single-vehicle run-off-road crashes. Technical report, NHTSA DOT HS 811 232, 2009.

[2] Cejun Liu and Tony Jianqiang Ye. Run-off-road crashes: An on-scene perspective. Technical report, NHTSA DOT HS 811 500, 2011.

[3] Y. Shibahata, K. Shimada, and T. Tomari. Improvement of vehicle maneuverability by direct yaw moment control. *Vehicle System Dynamics*, 22:465–481, 1993.

[4] AT van Zanten, R Erhardt, G Pfaff, and F Kost. Control aspects of the bosch-vdc. In *Proc. AVEC, Aachen*, 1996.

[5] Sergiy Antonov. *Model-based Vehicle Dynamics Control*. PhD thesis, Shaker Verlag, Aachen, 2008.

[6] Matthijs Klomp. *Longitudinal Force Distribution and Road Vehicle Handling*. PhD thesis, Chalmers University of Technology, Gothenburg, Sweden, 2010.

[7] Arman Nozad, Mathias Lidberg, Tim Gordon, and Matthijs Klomp. Optimal path recovery from terminal understeer. In *IAVSD Symposium, Manchester, UK*, 2011.

[8] Matthijs Klomp and Robert Thomson. Influence of front/rear drive force distribution on the lateral grip and understeer of all-wheel drive vehicles. *International Journal of Vehicle Design*, 56(1/2/3/4):34–48, 2011.

[9] Youssef A. Ghoneim, William C. Lin, David M. Sidlosky, Hsien H. Chen, Yuen-Kwok Chin, and Michael J. Tedrake. Integrated chassis control system to enhance vehicle stability. *International Journal of Vehicle Design*, 23:124–144, 2000.

[10] David Madås and Horace Lai. Test vehicle for regenerative braking emulation. Master's thesis, Chalmers University of Technology, Department of Applied Mechanics, Göteborg, Sweden, ISSN 1652-8557, 2011.

A VEHICLE DATA

The vehicle data shown in Table 1 that are used in the conducted simulations represent a mid-size passenger vehicle (Saab 9-3).

Description	Symb.	Value
Vehicle mass [kg]	m	1675
Yaw radius of gyration [m]	k	1.32
Wheel base [m]	l	2.675
Dist. from axle to CoG (f/r) [m]	l_1/l_2	$0.4l/0.6l$
Track width (f/r) [m]	w	1.5
Mass center height [m]	h	0.5
Lat. load transfer coeff. (f/r) [-]	ζ_{Y1}/ζ_{Y2}	0.17/0.16
Road friction coefficient [-]	μ_0	1
Axle friction coefficients (f/r) [-]	μ_1/μ_2	0.97/1.05

Table 1: Vehicle Data (Saab 9-3)